

Faraday patterns in coupled one-dimensional dipolar condensates

Kazimierz Lakomy,¹ Rejish Nath,² and Luis Santos¹

¹*Institut für Theoretische Physik, Leibniz Universität,
Hannover, Appelstrasse 2, D-30167, Hannover, Germany*

²*IQOQI and Institute for Theoretical Physics, University of Innsbruck, A-6020 Innsbruck, Austria*

(Dated: June 20, 2021)

We study Faraday patterns in quasi-one-dimensional dipolar Bose-Einstein condensates with parametrically driven dipolar interactions. We show that in the presence of a roton minimum in the excitation spectrum, the emergent Faraday waves differ substantially in two- and one-dimensional geometries, providing a clear example of the key role of confinement dimensionality in dipolar gases. Moreover, Faraday patterns constitute an excellent tool to study non-local effects in polar gases, as we illustrate for two parallel quasi-one-dimensional dipolar condensates. Non-local interactions between the condensates give rise to an excitation spectrum characterized by symmetric and anti-symmetric modes, even in the absence of hopping. We show that this feature, absent in non-dipolar gases, results in a critical driving frequency at which a marked transition occurs between correlated and anti-correlated Faraday patterns in the two condensates. Interestingly, at this critical frequency, the emergent Faraday pattern stems from a spontaneous symmetry breaking mechanism.

PACS numbers: 03.75.Kk, 89.75.Kd, 05.30.Jp

I. INTRODUCTION

Inter-particle interactions play an essential role in the physics of ultra-cold gases. Although in many experiments these interactions may be approximated by a contact potential, there is a rapidly growing interest in a novel type of cold gases in which electric or magnetic dipole-dipole interactions (DDI) are crucial for the occurring phenomena. These so-called dipolar gases include atoms with large magnetic moments [1–3], polar molecules [4–6] and Rydberg gases [7]. The distinct nature of the dipolar interactions leads to a wealth of novel physics, including a geometry-dependent stability and a roton-like minimum in the excitation spectrum (for reviews see e.g. [8, 9]).

Interestingly, the long-range dipolar interactions result in an inherent non-local nature of dipolar gases, particularly striking in deep optical lattices. For non-dipolar systems, gases trapped in different sites of a deep lattice do not interact with each other. Hence, for a vanishing inter-site hopping, different sites may be considered as independent, uncorrelated experiments. In contrast, inter-site DDI play a substantial role even in the absence of hopping. Recent lattice experiments have shown that the inter-site dipolar interactions are a key element in the dynamics [10], as well as in the stability and collapse of dipolar condensates [11, 12].

Faraday patterns constitute a paradigmatic example of pattern formation in periodically driven systems [13, 14] ranging from classical fluids [15], through multimode lasers [16] and superfluid Helium [17]. Interestingly, Faraday patterns may be observed in BECs by modulating the nonlinearity resulting from the interatomic interactions [18–23], as shown in recent experiments [24]. Faraday patterns in Bose-Einstein condensates (BECs) may be directly linked to the spectrum of elementary excitations, and in this sense provide an excellent insight

into fundamental properties of the condensates. In non-dipolar gases the Faraday pattern selection is determined uniquely for each modulation frequency due to the monotonically growing character of the excitation energy [25]. Interestingly, this is not anymore the case for dipolar BECs with a roton-like minimum in the excitation spectrum [26]. As a result, it has been shown that Faraday patterns in two-dimensional (2D) dipolar condensates present remarkable qualitative novel features [27]

In this paper, we analyze quasi-one-dimensional (quasi-1D) dipolar condensates with periodically driven dipolar interactions. We demonstrate that Faraday patterns provide a clear example of the non-trivial role of confinement dimensionality in dipolar gases, showing that in the presence of a roton-like minimum in the excitation spectrum, Faraday patterns in a quasi-1D trap differ significantly with respect to the 2D case [27]. Moreover, Faraday patterns provide as well an excellent tool for a study of non-local effects in dipolar condensates, as we illustrate with two parallel quasi-1D BECs, in the absence of tunneling. The non-local dipolar interactions between both BECs lead to an unfolding of the excitation spectrum into symmetric and anti-symmetric modes with respect to the transposition of the two condensates. We show that, as a consequence, at a critical driving frequency a transition between correlated (symmetric) and anti-correlated (anti-symmetric) Faraday patterns in the two BECs occurs. For the critical driving the emergent Faraday pattern differs from one realization to another, resulting from a spontaneous symmetry breaking mechanism.

The paper is structured as follows. In Sec. II we introduce the model for periodically driven quasi-1D dipolar condensates. Section III is devoted to Faraday patterns in a single quasi-1D BEC, with a focus on the differences as compared to 2D condensates. Section IV is dedicated to the effects of the inter-condensate dipolar interactions

on the Faraday pattern selection in two parallel disjoint quasi-1D dipolar condensates. We conclude in Sec. V.

II. MODEL

We consider in this paper quasi-1D dipolar BECs, either in a single trap (Sec. III) or in two parallel traps (Sec. IV). Since the former case may be considered as a particular realization of the latter, we present in this Section the general formalism for parallel quasi-1D BECs aligned along the z axis, and separated along the y axis by a distance Δ . We assume the potential barrier separating both quasi-1D BECs sufficiently large to suppress any hopping between them. Each condensate experiences a strong harmonic confinement of frequency ω_\perp in the x - y plane and no confinement along the z direction. The atoms possess a magnetic dipole moment μ (the results are equally valid for electric dipoles) oriented by an external field along the y axis. We employ dimensionless expressions, using units of frequency ω_\perp and length $l_\perp = \sqrt{\hbar/M\omega_\perp}$, with M the particle mass.

Due to the strong x - y confinement we assume that the system remains in the ground state of the x - y harmonic oscillator (this condition is self-consistently verified), and employ the non-local non-linear Schrödinger formalism developed in Refs. [28, 29] for a stack of quasi-1D dipolar BECs, to obtain the coupled equations for the wave functions $\psi_j(z)$ in traps $j = 1, 2$:

$$i\partial_t\psi_j(z) = \left[-\frac{1}{2}\partial_z^2 + gn_j(z) + \frac{2\pi}{3}g_d \sum_m \int dk_z e^{ik_z z} \hat{n}_m(k_z) F_{|m-j|}(k_z) \right] \psi_j(z). \quad (1)$$

Short-range interactions are characterized by the coupling constant $g = g^{3D}n_0/2\pi\hbar\omega_\perp l_\perp^3$, where n_0 is the linear density, and $g^{3D} = 4\pi a_{sc}\hbar^2/M$, with a_{sc} the s -wave scattering length. The DDI are determined by the coupling constant $g_d = g_d^{3D}n_0/2\pi\hbar\omega_\perp l_\perp^3$, where $g_d^{3D} = \mu_0\mu^2/4\pi$, with μ_0 the vacuum permeability. In Eq. (1), $\hat{n}_m(k_z) = |\psi_m(z)|^2$, and

$$F_p(k_z) = \int_0^\infty dk \frac{ke^{-\frac{1}{2}k^2}}{k^2 + k_z^2} \times [(k^2 - 2k_z^2) J_0(k\Delta p) - 3k^2 J_2(k\Delta p)], \quad (2)$$

where $J_n(x)$ are the Bessel functions of the first kind.

In the following we consider a parametric modulation of the dipole-dipole interactions

$$g_d(t) = \bar{g}_d(1 + 2\alpha \cos(2\omega t)), \quad (3)$$

where α characterizes the modulation strength. Such modulation may be implemented with intensity oscillations of the polarizing electric field for the case of polar

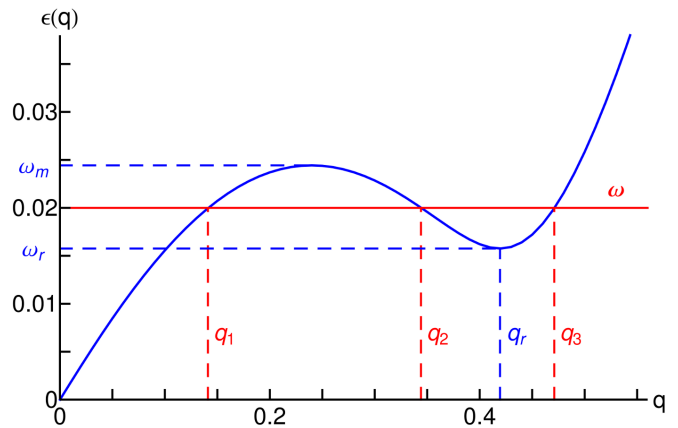


FIG. 1. (Color online) Excitation spectrum $\epsilon(q)$ of a single quasi-1D dipolar BEC, with $g = -0.1007$, $g_d = 0.0629$. Note the roton minimum at $\omega_r = \epsilon(q_r)$ and the maxon maximum at ω_m . For a driving frequency $\omega_r < \omega < \omega_m$ there are three possible momenta $q_{1,2,3}$ obeying the resonance condition $\epsilon(q) = \omega$.

molecules, or with additional transverse magnetic fields, which lead to a precession of the dipole moment orientation, for the case of magnetic dipoles.

The modulation of g_d induces Faraday waves. With the aim of examining the growth of such patterns, we introduce the following ansatz for the wave functions:

$$\psi_j(z, t) = \psi_{jH} (1 + A_j(t) \cos(qz)), \quad (4)$$

which describes well the physics of the pattern in the linear regime, where the modulation is weak and we may consider each momentum component q of the pattern separately. In Eq. (4), we introduce the complex amplitude $A_j(t) = u_j(t) + iv_j(t)$, which determines the perturbation from the initial homogeneous solution $\psi_{jH} = \exp\{-i\bar{\mu}_j[t + (\Omega_j/\omega) \sin(2\omega t)]\}$, where $\Omega_j = \alpha(1 - \bar{g}_d/\bar{\mu}_j)$, and $\bar{\mu}_j = g + \frac{2\pi}{3}\bar{g}_d \sum_m F_{|m-j|}(0)$ is the chemical potential. Inserting Eqs. (3) and (4), into Eq. (1), and linearizing in A_j we arrive at the system of equations describing the modulation dynamics

$$\frac{d^2 u_j}{dt^2} + \frac{q^2}{2} \left[\left(\frac{q^2}{2} + 2g \right) u_j + \frac{4\pi}{3} g_d(t) \sum_m u_m F_{|m-j|}(q) \right] = 0. \quad (5)$$

III. FARADAY PATTERNS IN A SINGLE QUASI-1D DIPOLAR BEC

We consider in this Section the case of a single condensate, being particularly interested in the differences between the emergent Faraday patterns in a quasi-1D trap and those predicted in Ref. [27] for a 2D condensate.

Employing a similar Bogoliubov analysis as the one presented in Ref. [28], we obtain the spectrum of elementary excitations in the considered case (see Fig. 1):

$$\epsilon(q) = \sqrt{\frac{q^2}{2} \left(\frac{q^2}{2} + 2g + \frac{4\pi}{3} g_d F_0(q) \right)} \quad (6)$$

where

$$F_0(q) = 1 + \frac{3}{2} q^2 e^{q^2/2} \text{Ei}(-q^2/2), \quad (7)$$

with $\text{Ei}(x)$ the exponential integral function. Using Eqs. (5) and (6), we arrive at the corresponding Mathieu equation [30]:

$$\frac{d^2 u}{dt^2} + [\epsilon^2(q) + 2\omega^2 b(q, \omega, \alpha) \cos(2\omega t)] u = 0 \quad (8)$$

with

$$b(q, \omega, \alpha) = \frac{2\pi}{3\omega^2} \bar{g}_d \alpha q^2 F_0(q). \quad (9)$$

Following Floquet theorem [31], the solutions of Eq. (8) are of the form $u(t) = e^{\tilde{\sigma}t} f(t)$ where $f(t) = f(t + \pi/\omega)$ and $\tilde{\sigma}(q, \omega, \alpha)$ is the Floquet characteristic exponent, which can be found numerically. If the real part $\sigma \equiv \text{Re}(\tilde{\sigma}) > 0$, the homogeneous quasi-1D BEC becomes dynamically unstable and Faraday patterns emerge. The typical wave length of the pattern will be determined by the most unstable mode, i.e., that with the largest σ . In the limit of small driving amplitude, $\alpha \rightarrow 0$, the properties of the pattern are governed by momenta q obeying parametric resonances $\epsilon_n(q) = n\omega$.

Contrary to non-dipolar BECs with a monotonic spectrum $\epsilon(q)$, dipolar gases may offer a more complex roton-maxon spectrum [26] (Fig. 1). As a consequence of this non-monotonic character, for a specific range of ω , between the roton and maxon frequencies (ω_r and ω_m , respectively) there are three values $q_1 < q_2 < q_3$ satisfying the resonance condition $\epsilon(q) = \omega$. Figure 2 shows the stability diagram for a driving frequency in this particular window. As expected, for small amplitudes α , the three instability tongues (white regions) correspond exactly to $q_{1,2,3}$ (Fig. 1). This opens an interesting question about which of the three modes dominates the pattern formation. For a 2D geometry, Ref. [27] showed that when modulating dipole-dipole interactions, the most unstable mode corresponds to the intermediate momentum $q_2 < q_r$, with q_r the roton momentum. Crucially, as we show below, this is not the case in a quasi-1D dipolar condensate. This striking contrast between quasi-1D and 2D predictions illustrates once more the key role played by the trapping geometry in dipolar gases.

The problem of the most unstable mode is best understood employing a series expansion of the Floquet exponent with small parameter $b(q, \omega, \alpha)$ [20, 32, 33], which, for the first parametric resonance $\epsilon(q) = \omega$, yields $\sigma \simeq b(q, \omega, \alpha)/2 \propto q^2 F_0(q)$. Remarkably, in contrast to

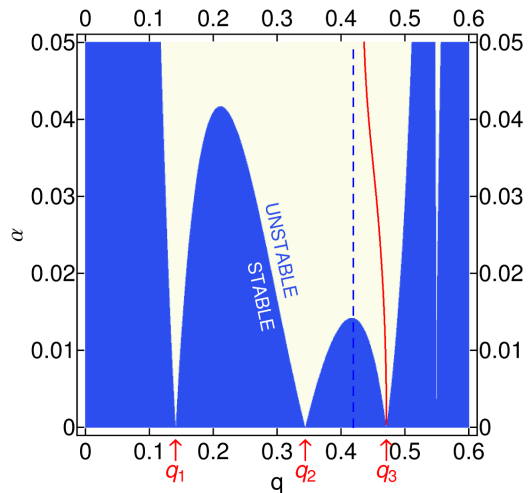


FIG. 2. (Color online) Stability diagram for the parameters of Fig. 1, as a function of the perturbation strength α and momentum q . The unstable region is depicted in white. The solid line indicates the most unstable mode, and the dashed line the roton momentum.

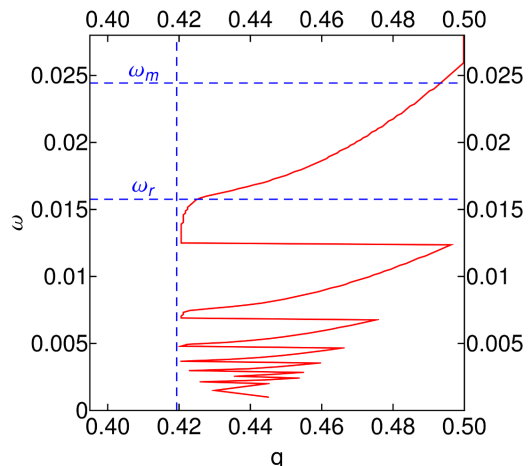


FIG. 3. (Color online) Most unstable momentum q as a function of the driving frequency ω for the parameters of Fig. 1, with $\alpha = 0.01$. The horizontal dashed lines indicate the roton and maxon frequencies ($\omega_{r,m}$), and the vertical line the roton momentum.

the 2D case, we find that the most unstable mode corresponds to the largest momentum $q_3 > q_r$ (solid line in Fig. 2). Fig. 3 depicts a momentum of the most unstable mode as a function of the driving frequency ω . The plot confirms that for all frequencies within the window $\omega_m < \omega < \omega_r$ the momentum characterizing the most unstable mode is larger than the roton momentum, contradicting the prediction for a 2D pancake geometry [27]. For $\omega < \omega_r$, alike in the 2D case, the observed modulations are dominated by higher resonances with q in the vicinity of q_r . However, unlike the 2D scenario, even in this regime the most unstable mode in a quasi-1D BEC is characterized by $q > q_r$. We emphasize that the different

nature of the Faraday pattern reported here stems solely from the quasi-1D character of the condensate, which leads to a specific momentum dependence of $b(q, \omega, \alpha)$ that differs from that in 2D.

We have simulated numerically the time evolution of the non-local non-linear Schrödinger equation (1) with the parametrically driven nonlinearity, according to Eq. (3). The emergent pattern has been examined by means of Fourier transform of the condensate density, which confirmed the results for the most unstable mode that we obtained within the Mathieu analysis.

IV. FARADAY PATTERNS IN TWO 1D DIPOLAR BECs

We now turn to the study of Faraday patterns in two parallel quasi-1D dipolar BECs. For non-dipolar BECs, in the absence of hopping, each BEC behaves independently, and hence an experiment with two BECs reduces to two uncorrelated experiments with a single condensate. The situation is radically different in dipolar BECs, since, despite the absence of hopping, the non-local character of the dipolar potential gives rise to a coupling between the two BECs, with the strength of the inter-condensate interactions governed by $F_1(k_z)$. These non-local interactions lead to a collective character of the elementary excitations that are shared among the two quasi-1D condensates [28, 34]. Consequently, the excitation spectrum unfolds into two branches

$$\epsilon_{\pm}(q) = \sqrt{\frac{q^2}{2} \left(\frac{q^2}{2} + 2g + \frac{4\pi}{3} g_d (F_0(q) \pm F_1(q)) \right)}, \quad (10)$$

which correspond, respectively, to symmetric and anti-symmetric states with respect to the transposition of traps $j = 1 \leftrightarrow j = 2$.

Interestingly, this implies that a periodic modulation of the dipolar interactions yields two different parametric resonances for each driving frequency $\omega = \epsilon_{\pm}(q_{\pm})$, even in the absence of the roton minimum (see Fig. 4). Note, that the patterns are characterized not only by their momentum q_{\pm} but also by their symmetric (+) or anti-symmetric (-) character. In analogy to Sec. III, the double solution raises a fundamental question about which of these two modes is the most unstable, and hence provides the dominant Faraday pattern. We stress that this non-trivial physics stems directly from the inter-condensate interactions, which lead to the splitting between the two branches in the spectrum, being a qualitatively new feature of dipolar condensates.

Similarly to the previous section, we employ Eqs. (5) for $j = 1, 2$, and the spectra (10). In turn, we obtain two decoupled Mathieu equations for the symmetric and anti-symmetric combinations $u_{\pm} = u_1 \pm u_2$:

$$\frac{d^2 u_{\pm}}{dt^2} + [\epsilon_{\pm}^2(q) + 2\omega^2 b_{\pm}(q, \omega, \alpha) \cos(2\omega t)] u = 0 \quad (11)$$

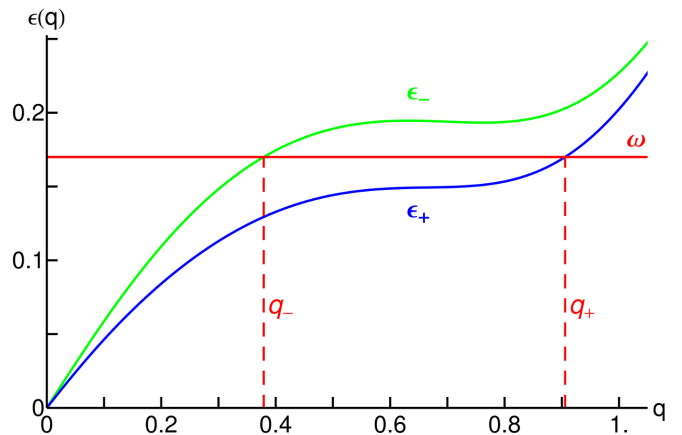


FIG. 4. (Color online) Elementary excitations of two parallel quasi-1D dipolar BECs, for $g = -0.0629$, $\bar{g}_d = 0.1749$, and $\Delta/l_{\perp} = 6$. Note the two branches of the elementary excitations $\epsilon_{\pm}(q)$, corresponding, respectively, to symmetric and anti-symmetric modes with respect to the transposition of traps $j = 1 \leftrightarrow j = 2$.

with

$$b_{\pm}(q, \omega, \alpha) = \frac{2\pi}{3\omega^2} \bar{g}_d \alpha q^2 (F_0(q) \pm F_1(q)), \quad (12)$$

to which we apply the Floquet analysis employed in the study of Eq. (8). As in the case of a single BEC, the first parametric resonances $\epsilon_{\pm}(q_{\pm}) = \omega$ are characterized by the Floquet exponent $\sigma_{\pm} \simeq b_{\pm}(q, \omega, \alpha)/2 \propto q^2 (F_0(q) \pm F_1(q))$, and the emerging Faraday pattern is determined, for each driving frequency separately, by the mode with the largest σ . Remarkably, the involved mo-

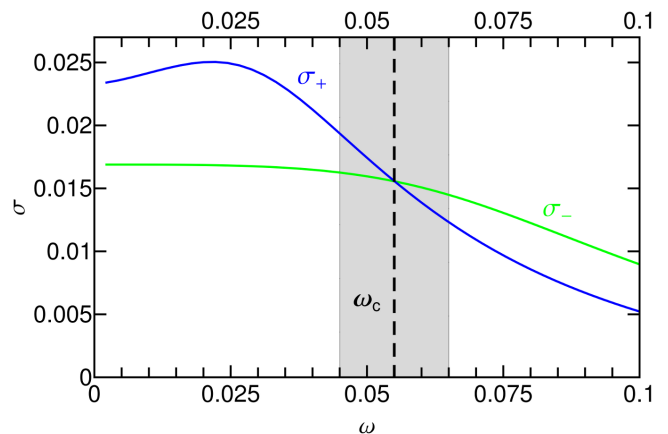


FIG. 5. (Color online) Real part σ_{\pm} of the Floquet exponent, corresponding to the the first parametric resonance for the symmetric and anti-symmetric excitation branches $\epsilon_{\pm}(q) = \omega$, as a function of the driving frequency ω . Note that at a critical frequency $\omega_c = 0.055$, both exponents are equal, $\sigma_+ = \sigma_-$, indicating a transition between the symmetric and the anti-symmetric Faraday pattern. In the figure we employ $g = -0.0435$, $\bar{g}_d = 0.0437$, $\Delta = 6l_{\perp}$, and $\alpha = 0.02$.

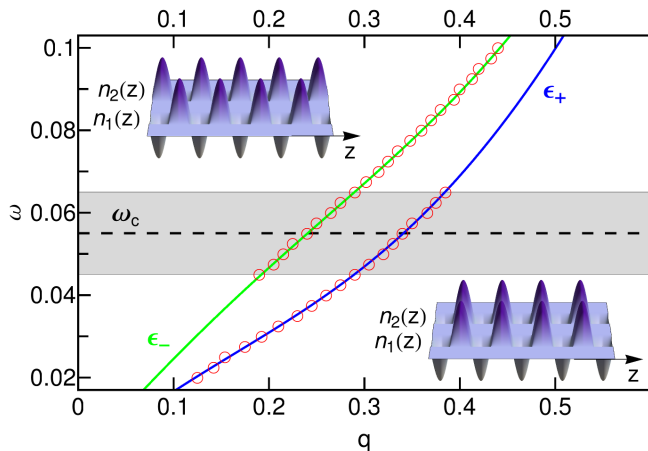


FIG. 6. (Color online) Analysis of the pattern selection as a function of the driving frequency ω , in the neighborhood of the critical frequency ω_c (for the same parameters as in Fig. 5). The solid lines represent the excitation branches. For each ω we indicate with a circle a momentum value where the numerical Fourier transform $\hat{n}_j(k_z)$ of the Faraday pattern shows a clear maximum. For ω well below (above) ω_c we observe a single peak at q_+ (q_-) indicating that a symmetric (anti-symmetric) Faraday pattern emerges (see insets). In the vicinity of ω_c (shaded region), both modes are equally unstable and we observe the two corresponding peaks occurring simultaneously in the Fourier transform (see text).

mentum dependence of $F_0(q) \pm F_1(q)$ leads to an intricate relation between the Floquet exponents and the driving frequency ω , as presented in Fig. 5.

Crucially, the curves $\sigma_{\pm}(\omega)$ cross at a critical frequency ω_c . In consequence, we expect a distinct transition, as a function of the driving frequency ω , between the symmetric Faraday pattern for $\omega < \omega_c$ and the anti-symmetric pattern for $\omega > \omega_c$. Such transition is marked by an abrupt change of the patterns from a maximum-maximum alignment (correlated patterns) to a maximum-minimum alignment (anti-correlated patterns), as depicted in the corresponding insets of Figs. 6 and 7. Moreover, for $\omega = \omega_c$ the patterns in both condensates exhibit a pronounced change of the wavelength of the modulation, from $1/q_+(\omega_c)$ to $1/q_-(\omega_c)$.

This transition has been confirmed by means of direct numerical simulations of Eqs. (1), with the parametric driving governed by Eq. (3). As for a single condensate, we Fourier transform the density of each condensate to obtain the dominant momenta of the emergent Faraday patterns. The results, in the vicinity of the critical frequency ω_c , are depicted in Fig. 6, where, on top of the spectra ϵ_{\pm} , for each driving frequency ω we indicate with a circle the momentum value where the numerically evaluated $\hat{n}_j(k_z)$ shows a marked maximum. We find that, in agreement with the results for $\sigma_{\pm}(\omega)$ presented in Fig. 5, for ω well below ω_c the pattern presents a single momentum component at q_+ , being characterized by a corre-

lation between the patterns in both quasi-1D BECs. In contrast, for ω well above ω_c a single momentum component q_- is observed, and the patterns in the two quasi-1D BECs are anti-correlated.

In order to quantify the transition between correlated and anti-correlated patterns we introduce the correlation coefficient

$$r = \frac{\int dz S_{n_1}(z) \cdot S_{n_2}(z)}{\sqrt{\int dz S_{n_1}^2(z)} \cdot \sqrt{\int dz S_{n_2}^2(z)}}, \quad (13)$$

where $S_{n_j}(z) = n_j(z) - \bar{n}_j$, with \bar{n}_j the average density in a trap j . Pattern correlation is then characterized by $r > 0$, whereas anti-correlation leads to $r < 0$. Fig. 7 illustrates the radically different time evolution of the correlation coefficient below and above the critical driving ω_c . Clearly, for frequencies sufficiently smaller (larger) than ω_c the system arrives at perfectly correlated (anti-correlated) pattern with $|r| = 1$.

An interesting scenario occurs for driving frequencies in the vicinity of the critical ω_c (shaded region in Figs. 5 and 6), where both the symmetric pattern with wavelength $1/q_+(\omega_c)$ and the anti-symmetric pattern with wavelength $1/q_-(\omega_c)$ are equally unstable. As a result, the Fourier transform of the density in each quasi-1D BEC shows a simultaneous appearance of both momentum peaks, q_+ and q_- (see Fig. 6).

Note that at $\omega = \omega_c$, not only $\epsilon_+(q_+) = \epsilon_-(q_-)$ but also $b_+(q_+, \omega, \alpha) = b_-(q_-, \omega, \alpha)$ and hence the two Mathieu equations (11) for u_+ and u_- become identical. This

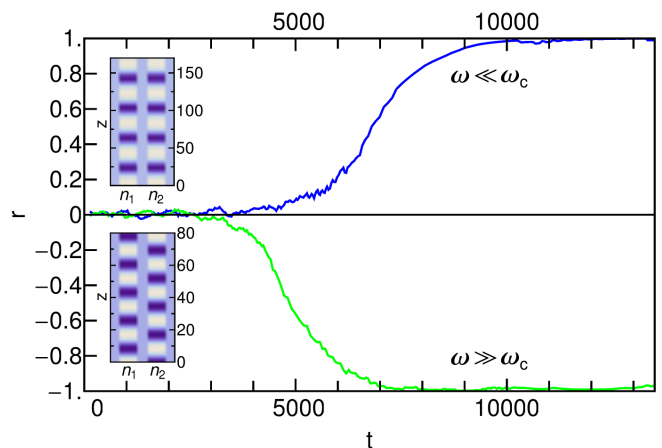


FIG. 7. (Color online) Correlation function $r(t)$ for the same parameters as in Fig. 6 ($\omega_c = 0.055$). The upper curve, which corresponds to $\omega = 0.025 < \omega_c$, approaches $r = 1$ indicating a perfectly correlated pattern in both quasi-1D traps. The lower curve, which corresponds to $\omega = 0.08 > \omega_c$, reaches $r = -1$ proving a perfect anti-correlation between the Faraday patterns in the two traps. The insets show the corresponding numerical results for the density distribution $n_j(z)$ for $t = 11000$, with the bright (dark) colors indicating density maxima (minima). Naturally, for sufficiently long times, well beyond the linear regime, the Faraday patterns and their correlations are eventually destroyed.

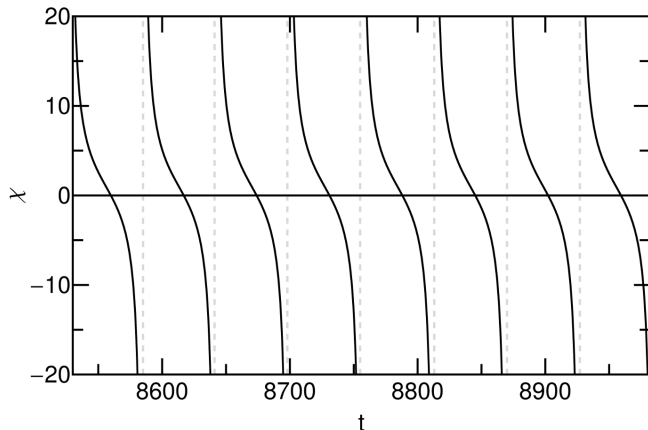


FIG. 8. (Color online) Population imbalance $\chi(t)$ between the two peaks at $q_{\pm}(\omega_c)$ for the critical driving $\omega = \omega_c$ (for the same parameters as Fig. 6). Note the 2ω periodicity ($T = \pi/\omega = 57.1$) that stems from a spontaneous symmetry breaking mechanism (see text).

symmetry is however spontaneously broken in experiments due to quantum and thermal fluctuations, which lead to different initial conditions (populations) for both modes, that change randomly from one realization to another. This spontaneous symmetry breaking mechanism is best studied quantitatively by considering the relative weight of the momentum peaks at q_+ and q_- in the Fourier-transform of the density $\hat{n}(k_z)$. To this end, we define the imbalance parameter

$$\chi(t) = \frac{\hat{n}(q_+, t) - \hat{n}(q_-, t)}{\hat{n}(q_+, t) + \hat{n}(q_-, t)}. \quad (14)$$

For ω well below or above ω_c , once the pattern emerges, $\chi(t) = \pm 1$. In the vicinity of ω_c , however, the imbalance parameter $\chi(t)$ shows a clear periodicity with frequency 2ω (see Fig. 8). Note that these oscillations do not result from non-linear competition, as they occur well within the linear regime. In fact, the 2ω oscillations

of $\chi(t)$ originate in different, spontaneously chosen, initial conditions for u_+ and u_- , which lead to their different time evolution that can be well approximated by $u_{\pm}(t) = (u_{\pm}^c \cos(\omega t) + u_{\pm}^s \sin(\omega t)) \exp(\sigma \omega t)$, where $u_{\pm}^{c/s}$ are the constants determined by the initial conditions. Furthermore, spontaneous symmetry-breaking leads to a different result for the imbalance $\chi(t)$ from one realization to another, what we have confirmed by considering small random differences in the initial conditions for our numerical simulations of Eqs. (1).

V. CONCLUSIONS

Faraday patterns in dipolar BECs are crucially dependent on the unique properties of the dipole-dipole interactions. In particular, due to the long-range anisotropic nature of the dipolar interactions, the character of the Faraday patterns depends strongly on the dimensionality of the condensates. We have shown that for periodically modulated dipolar interactions, Faraday patterns in 2D and 1D geometries differ substantially in the presence of a roton minimum in the excitation spectrum. Moreover, for parallel quasi-1D dipolar BECs, the inter-condensate interactions lead, even in the absence of hopping, to an excitation spectrum characterized by symmetric and anti-symmetric modes. This, in turn, gives rise at a critical driving frequency to a marked transition between correlated and anti-correlated Faraday patterns in the two condensates. Interestingly, at this transition point the Faraday pattern selection stems from a spontaneous symmetry breaking mechanism.

VI. ACKNOWLEDGEMENT

We acknowledge funding by the German-Israeli Foundation, the Cluster of Excellence QUEST and the DFG (SA1031/6).

-
- [1] A. Griesmaier, J. Werner, S. Hensler, J. Stuhler, and T. Pfau, *Phys. Rev. Lett.* **94**, 160401 (2005).
 - [2] M. Lu, N. Q. Burdick, S. H. Youn, and B. L. Lev, *Phys. Rev. Lett.* **107**, 190401 (2011).
 - [3] K. Aikawa, A. Frisch, M. Mark, S. Baier, A. Rietzler, R. Grimm, and F. Ferlaino, *Phys. Rev. Lett.* **108**, 210401 (2012).
 - [4] J. Deiglmayr, A. Grochola, M. Repp, K. Mörtilbauer, C. Glück, J. Lange, O. Dulieu, R. Wester, and M. Weidemüller, *Phys. Rev. Lett.* **101**, 133004 (2008).
 - [5] K.-K. Ni, S. Ospelkaus, D. Wang, G. Quémener, B. Neyenhuis, M. H. G. de Miranda, J. L. Bohn, J. Ye, and D. S. Jin, *Nature* **464**, 1324 (2010).
 - [6] S. Ospelkaus, K.-K. Ni, G. Quémener, B. Neyenhuis, D. Wang, M. H. G. de Miranda, J. L. Bohn, J. Ye, and D. S. Jin, *Phys. Rev. Lett.* **104**, 030402 (2010).
 - [7] D. Tong, S. M. Farooqi, J. Stanojevic, S. Krishnan, Y. P. Zhang, R. Côté, E. E. Eyler, and P. L. Gould, *Phys. Rev. Lett.* **93**, 063001 (2004).
 - [8] M. Baranov, *Phys. Rep.* **464**, 71 (2008).
 - [9] T. Lahaye, C. Menotti, L. Santos, M. Lewenstein, and T. Pfau, *Rep. Prog. Phys.* **72**, 126401 (2009).
 - [10] M. Fattori, G. Roati, B. Deissler, C. D’Errico, M. Zaccanti, M. Jona-Lasinio, L. Santos, M. Inguscio, and G. Modugno, *Phys. Rev. Lett.* **101**, 190405 (2008).
 - [11] S. Müller, J. Billy, E. A. L. Henn, H. Kadau, A. Griesmaier, M. Jona-Lasinio, L. Santos, and T. Pfau, *Phys. Rev. A* **84**, 053601 (2011).
 - [12] J. Billy, A. L. Henn, S. Müller, T. Maier, H. Kadau, A. Griesmaier, M. Jona-Lasinio, L. Santos, and T. Pfau,

- arXiv:1205.5176.
- [13] M. Faraday, *Phil. Trans. R. Soc. Lond.* **121**, 299 (1831).
 - [14] M. C. Cross and P. C. Hohenberg, *Rev. Mod. Phys.* **65**, 851 (1993).
 - [15] D. Binks and W. van de Water, *Phys. Rev. Lett.* **78**, 4043 (1997).
 - [16] C. Szwaj, S. Bielawski, D. Derozier, and T. Erneux, *Phys. Rev. Lett.* **80**, 3968 (1998).
 - [17] H. Abe, T. Ueda, M. Morikawa, Y. Saitoh, R. Nomura, and Y. Okuda, *Phys. Rev. E* **76**, 046305 (2007).
 - [18] K. Staliunas, S. Longhi, and G. J. de Valcárcel, *Phys. Rev. Lett.* **89**, 210406 (2002).
 - [19] K. Staliunas, S. Longhi, and G. J. de Valcárcel, *Phys. Rev. A* **70**, 011601 (2004).
 - [20] A. I. Nicolin, R. Carretero-González, and P. G. Kevrekidis, *Phys. Rev. A* **76**, 063609 (2007).
 - [21] A. I. Nicolin, *Phys. Rev. E* **84**, 056202 (2011).
 - [22] A. I. Nicolin, *Physica A* **391**, 1062 (2012).
 - [23] A. Balaž and A. I. Nicolin, *Phys. Rev. A* **85**, 023613 (2012).
 - [24] P. Engels, C. Atherton, and M. A. Hofer, *Phys. Rev. Lett.* **98**, 095301 (2007).
 - [25] M. Modugno, C. Tozzo, and F. Dalfovo, *Phys. Rev. A* **74**, 061601 (2006).
 - [26] L. Santos, G. V. Shlyapnikov, and M. Lewenstein, *Phys. Rev. Lett.* **90**, 250403 (2003).
 - [27] R. Nath and L. Santos, *Phys. Rev. A* **81**, 033626 (2010).
 - [28] K. Lakomy, R. Nath, and L. Santos, *Phys. Rev. A* **85**, 033618 (2012).
 - [29] K. Lakomy, R. Nath, and L. Santos, *Phys. Rev. A* **86**, 013610 (2012).
 - [30] N. W. McLachlan, *Theory and applications of Mathieu functions* (Clarendon Press, 1947).
 - [31] P. M. Morse and H. Feshbach, *Methods of Theoretical Physics, Part I* (McGraw-Hill, New York, 1953).
 - [32] F. Tisserand, *Traité de Mécanique Celeste, Tome III* (Paris, Gauthier-Villars et fils, 1894).
 - [33] A. I. Nicolin, *Mode-locking, Faraday patterns and the variational approach to Bose-Einstein-condensed gases*, Ph.D. thesis, The Niels Bohr Institute, Copenhagen, Denmark (2008).
 - [34] M. Klawunn and L. Santos, *Phys. Rev. A* **80**, 013611 (2009).